Methodology for Processing Seismograms Containing Total Internal Reflections

Erick Baziw, *Senior Member, IEEE*, and Gerald Verbeek

***Abstract*—A very common problem encountered in downhole seismic testing (DST) and crosshole seismic testing (CST) is the processing of seismograms that contain total internal reflections (TIRs). TIRs arise when the incident angle exceeds the critical angle, and they are associated with reflected source wave distortions due to the fact that the reflection coefficients become complex. TIRs are typical in CST investigations (since horizontally traveling source waves have high angles of incidence on bounding stratigraphic layers), whereas in DST investigations, TIRs are encountered whenever there are significant man-made structures (piles, stone columns, and deep underground structures such as deep basements, parking garages, and dam structures). To process seismograms containing TIRs, time-variant blind seismic deconvolution (BSDtv) techniques are required, and this paper outlines a new formulation of a previously published concept in blind seismic deconvolution referred to as principle phase decomposition (PPD). This new PPD filter formulation allows for BSDtv where the direct source wave is isolated from the reflected source waves. The BSDtv PPD filter formulation is referred to as BSDSolver-tv.**

***Index Terms*—Deconvolution, iterative methods, Kalman filtering, Monte Carlo methods, parameter estimation, reflection, seismic signal processing, state estimation, time-varying filters.**

I. Introduction

ACCURATE *in situ* P- and S-wave velocity profiles are essential in geotechnical foundation designs. These parameters are used in both static and dynamic soil analyses where the elastic constants are input variables into the models defining the different states of deformations, such as elastic, elastoplastic, and failure [1]. Equation (1) illustrates the relationship between the elastic constants of Poisson's ratio ν, shear modulus G_0, Young's modulus E, and bulk modulus B, with the compression wave velocity V_P and the shear wave velocity V_S. Thus

$$\begin{aligned} \nu &= \frac{V_P^2 - 2V_S^2}{\left(V_P^2 - V_S^2\right)^2} \\ G_0 &= \rho V_S^2 \\ E &= 2G_0(1+\nu) \\ B &= \frac{E}{3(1-2\nu)} \end{aligned} \tag{1}$$

where ρ is the mass density of the soil.

The shear wave velocity is also an important parameter for evaluating liquefaction potential due to the fact that it is influenced by many of the same variables that influence liquefaction (e.g., void ratio, soil density, confining stress, stress history, and geologic age). As stated by Andrus *et al.* [2], "predicting the liquefaction resistance of soil is an important step in the engineering design of new structures and the retrofit of existing structures in earthquake prone regions." Aki and Richards [3] also outlined that the amplitude of ground motion[1] should depend on the density and the shear wave velocity of near-surface soils and rocks, according to the theory of wave propagation. Since the change in density with the increase in depth is relatively minor compared with that of the shear wave velocity, the latter is a very useful parameter to represent site conditions [4], and therefore, the near-surface shear wave velocity values are utilized for site characterization in calculating seismic hazards.

The downhole seismic test (DST) such as the seismic cone penetration test (SCPT) [5], [6] and the crosshole seismic test (CST) [7][2] are geotechnical *in situ* site characterization tools with which V_S and V_P can be accurately estimated. In DST and CST, the velocities are determined by obtaining the corresponding source wave relative arrival times as the source wave travels within the stratigraphic profile. This is typically done by identifying reference points or markers within the seismograms (e.g., maximum peaks/troughs or crossovers) [8], [9] or through techniques that implement the cross-correlation function or the cross-power spectrum [6], [10]. For example, Fig. 1 illustrates the time markers of 2, C, 3, and D (first peak, first crossover, second peak, and second crossover, respectively) for reversely polarized traces simulated for a DST. For these approaches, it is obviously of paramount importance to have high-quality first-arriving source waves from each recorded trace so that meaningful relative arrival times are obtained.

Once the relative arrival times are derived, the standard industry practice is then to assume straight ray travel paths between seismic source and receiver. In this case, the *in situ* velocities are calculated as the ratio between the relative arrival time differences and the corresponding relative travel path differences between successive depths (see Fig. 2 for DST) or lateral offsets (see Fig. 3 for CST) (i.e., $V = \Delta d/\Delta T$, where ΔT is the relative arrival time difference, Δd is the relative

Manuscript received October 18, 2013; revised December 17, 2013; accepted February 14, 2014.

E. Baziw was with The University of British Columbia, Vancouver, BC V6T 1Z4, Canada. He is now with Baziw Consulting Engineers Ltd., Vancouver, BC V6S 1Z4, Canada.

G. Verbeek was with the University of Texas at Tyler, Tyler, TX 75799 USA.

Color versions of one or more of the figures in this paper are available online at http://ieeexplore.ieee.org.

Digital Object Identifier 10.1109/TGRS.2014.2307071

[1] Amplification is defined as an in increase in seismic ground motion intensity greater than that expected for firm ground or rock. Susceptibility is defined as the propensity for ground motion amplification to occur.

[2] ASTM standards D7400-08 and D4428/D4428M-07 provide thorough outlines of the DST and CST equipment and methodologies, respectively.

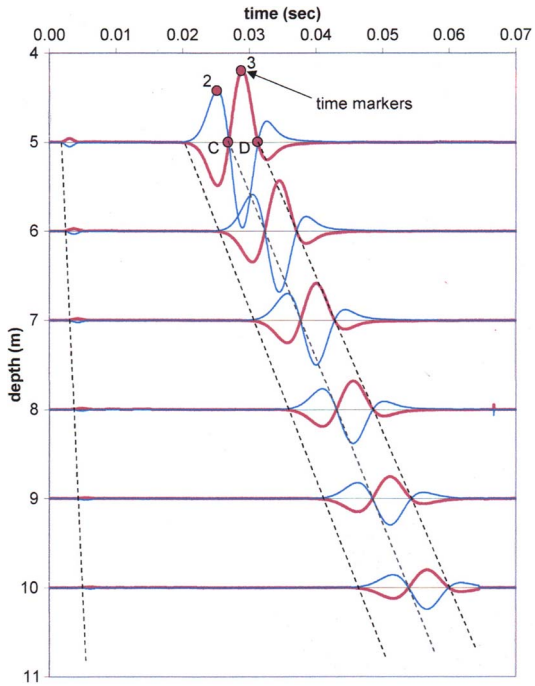

Fig. 1. Typical DST time markers [8].

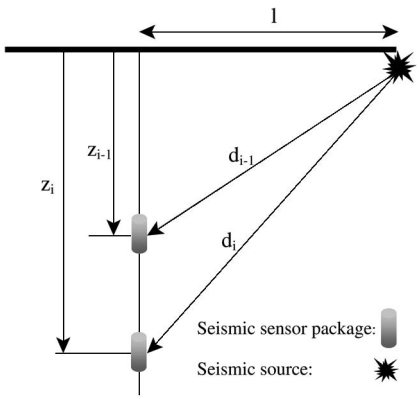

Fig. 2. Schematic of the typical DST configuration [10].

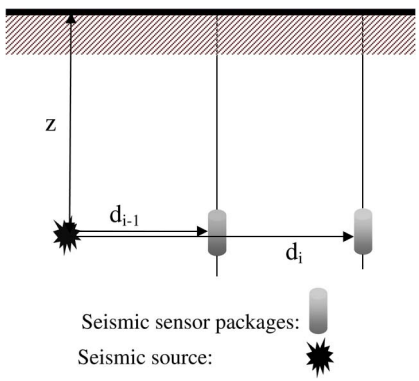

Fig. 3. Schematic of the typical CST configuration [10].

travel path difference, and V is the corresponding interval velocity). Baziw [11], [12] and Baziw and Verbeek [13] outlined a more sophisticated DST approach in obtaining *in situ* V_S and V_P velocities from relative arrival times. In this technique, an iterative forward modeling (IFM) method is utilized, which takes into account source wave refraction as the source travels within the stratigraphic profile.

However, in both the DST and CST investigations, there are site conditions that result in wave multiples referred to as total internal reflections (TIRs), which make the estimation of interval relative arrival times a very difficult, if not impossible, task. TIRs are typical in CST investigations (since horizontally traveling source waves have high angles of incidence on bounding stratigraphic layers), whereas in DST investigations, TIRs are encountered whenever there are significant man-made structures nearby the test location (e.g., foundation piles, stone columns, or deep underground structures such as deep basements, parking garages, and dam structures).

II. Background

A. TIRs

Baziw and Verbeek [10] gave a detailed outline and description of TIRs. For completeness, a review of TIRs is given along with simulated examples. Whenever angles of incidents exceed the critical angle, TIRs occur, and they are commonly incurred during downhole and crosshole seismic testing and result in source wave distortions due to the fact that the reflection coefficients become complex.

Seismic sources for engineering investigations are often designed to generate either dominantly P- and SV-waves or dominantly SH-waves due to the fundamentally different behavior of P-, SV-, and SH-waves at a boundary. When a P- or an SV-wave strikes a boundary, four outgoing waves are generated (SV and P, both reflected and transmitted), whereas an SH-wave will only generate two outgoing waves (reflected and transmitted SH-waves), thus simplifying the recorded seismic time series. A popular SH source is the hammer beam, which consists of applying a hammer blow laterally to the sides of specially designed plates fixed at the surface. The particle motion of an SH-wave occurs within the horizontal plane and is orthogonal to the ray path. Fig. 4 outlines a schematic of the SH-wave SCPT investigation that is being carried out, where the SH-wave velocity of the piles/stone columns (V2) is much greater than that of the surrounding soil (V1).

In Fig. 4, ρ is the medium density; **2** denotes the first-arriving direct SH source wave; **1**, **3**, **4**, and **5** denote the reflecting waves; $\times$ denotes the SH-wave particle motion (in and out on the horizontal plane); θ_1 denotes the incident and reflecting angles; $\beta_1 = 90^\circ - \theta_1$; and θ_2 is the refraction angle. Referring to Fig. 4 and using the kinematic boundary conditions, which require that the displacement be continuous across the interface of the media, the *precritical reflection coefficient* (reflections at angles less than the critical angle) is

$$R = \frac{A_1}{A_0} = \frac{G_1\eta_1 - G_2\eta_2}{G_1\eta_1 + G_2\eta_2} = \frac{\rho_1 V_1 \cos\theta_1 - \rho_2 V_2 \cos\theta_2}{\rho_1 V_1 \cos\theta_1 + \rho_2 V_2 \cos\theta_2}. \quad (2)$$

The *postcritical reflection coefficient can be then* given as

$$R = \frac{A_1}{A_0} = \frac{G_1\acute{\eta}_1 - iG_2\acute{\eta}_2}{G_1\acute{\eta}_1 + iG_2\acute{\eta}_2} = \frac{e^{-i\alpha}}{e^{+i\alpha}} = e^{-i2\alpha} \quad (3)$$

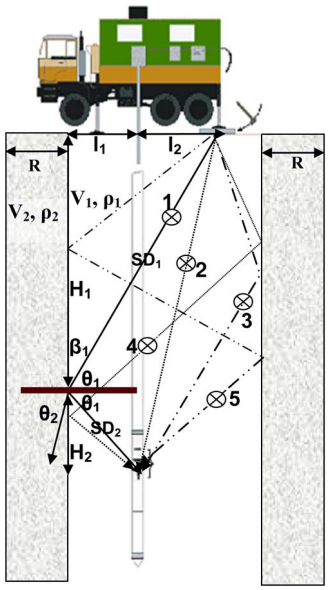

Fig. 4. Cross section of SCPT illustrating direct and reflecting source waves.

with

$$\alpha = \tan^{-1}\left(\frac{G_2\acute{\eta}_2}{G_1\acute{\eta}_1}\right) \tag{4}$$

where R is the reflection coefficient; A_0 is the amplitude of incident wave, A_1 is the amplitude of reflected wave; G_1 and G_2 are the shear moduli of media 1 and 2, respectively; i is the imaginary number; and $\acute{\eta}_1$ and $\acute{\eta}_2$ are the *postcritical* horizontal slowness within media 1 and 2, respectively, which can be defined as follows:

$$\acute{\eta}_1 = \sqrt{u_1^2 - p^2} \tag{5a}$$

$$\acute{\eta}_2 = \sqrt{p^2 - u_2^2} \tag{5b}$$

where p is the ray parameter, $u_1 = 1/V_1$, and $u_2 = 1/V_2$. The ray parameter represents the apparent slowness of the wavefront along the interface between media 1 and 2.

The seismogram for TIRs is generated by convolving the source waves by the reflection coefficients given in (3) for various incident angles that exceed the critical angle. In the frequency domain, this is equivalent to multiplying the source wave by the reflection coefficients given by (3), producing a frequency-independent phase shift as shown in the following:

$$\begin{aligned} U &= RA_0e^{i(kx-\omega t)} \\ &= A_0e^{-i2\alpha}e^{i(kx-\omega t)} \\ &= A_0e^{i(kx-\omega(t+2\alpha/\omega))} \end{aligned} \tag{6}$$

where parameter U represents the displacement of the reflected wave, k represents the wavenumber, x represents the distance, ω represents the angular frequency, and t represents the time. As evident in (6), the reflected wave has a phase shift of $2\alpha/\omega$ or $2\alpha/2\pi f_d$, where f_d is the dominant frequency of the source wave.

It should be noted that the displacement field generated by a single body force contains both *near-field* and *far-field* terms, with the *near-field* terms proportional to r^2, whereas the *far-field* terms decay as r^{-1}, where r is the travel distance from the source to the receiver [3]. Irrespective of whether the *near-field* or the *far-field* term is reflected at the *postcritical* angle, the reflected wave will have a phase shift according to (3).

It is shown [3] that any phase shift of a source wave can be determined from the source wave and its Hilbert transform as follows:

$$\hat{y}(t) = \cos\alpha y(t) + \sin\alpha \mathrm{H}\left[y(t)\right] \tag{7}$$

where $\hat{y}(t)$ is the phase-shifted source wave, $y(t)$ is the original source wave, α is the phase shift, and $H[y(t)]$ is the Hilbert transform of the source wave, which introduces a 90° phase shift of a function [i.e., $R = -i$ in (3)].

A commonly utilized analytical source wave in seismic signal processing is the Ricker source wave. The Ricker wavelet is represented in the time domain as [14]

$$\mathrm{RW}(t) = A_0\left(1-2\pi^2 f_d^2(t-t_0)^2\right)\exp^{-\pi^2 f_d^2(t-t_0)^2}, \quad t \le t_0 \tag{8}$$

where A_0 is the wavelet maximum amplitude (centered between two flanking lobes), f_d is the dominant or the peak frequency of the Ricker wavelet, and t_0 is the source wave arrival time of maximum amplitude.

To provide illustrative examples of the phase shifting of seismic source waves due to TIRs, (7) was applied on the Ricker source waves. In Fig. 5(a)–(d), the solid lines represent a Ricker source wave with a dominant frequency of 50 Hz. The dotted lines in Fig. 5(a)–(d) are the inputted Ricker source wave phase shifted by 40°, 90°, 120°, and 220°, respectively. As demonstrated in these figures, although the dominant frequency has been retained and the arrival time has remained the same, the source waves have been phase shifted within the envelope of the wave packet, and the minimum and maximum peaks have been modified.

This impact of the phase shift introduces a significant seismic signal processing challenge that is best addressed by applying a blind seismic deconvolution (BSD) technique that allows for time-variant source waves.

B. BSD and BSDtv

Seismic deconvolution is one of the most widely researched and implemented seismic signal processing tools [15]–[18]. The primary goal of seismic deconvolution is to remove the characteristics of the source wave from the recorded seismic time series, so that one is ideally left with only the reflection coefficients. These reflection coefficients identify and quantify the impedance mismatches between different geological layers, which are of great interest not only when exploring for minerals and oil and gas reserves but also when constructing civil structures and their associated foundations and monitoring the integrity of earth dams.

In seismology, the recorded time series $z(t)$ is defined as the linear convolution of the source wave $S(t)$, with the Earth's reflection coefficients $\mu(t)$, with additive measurement noise

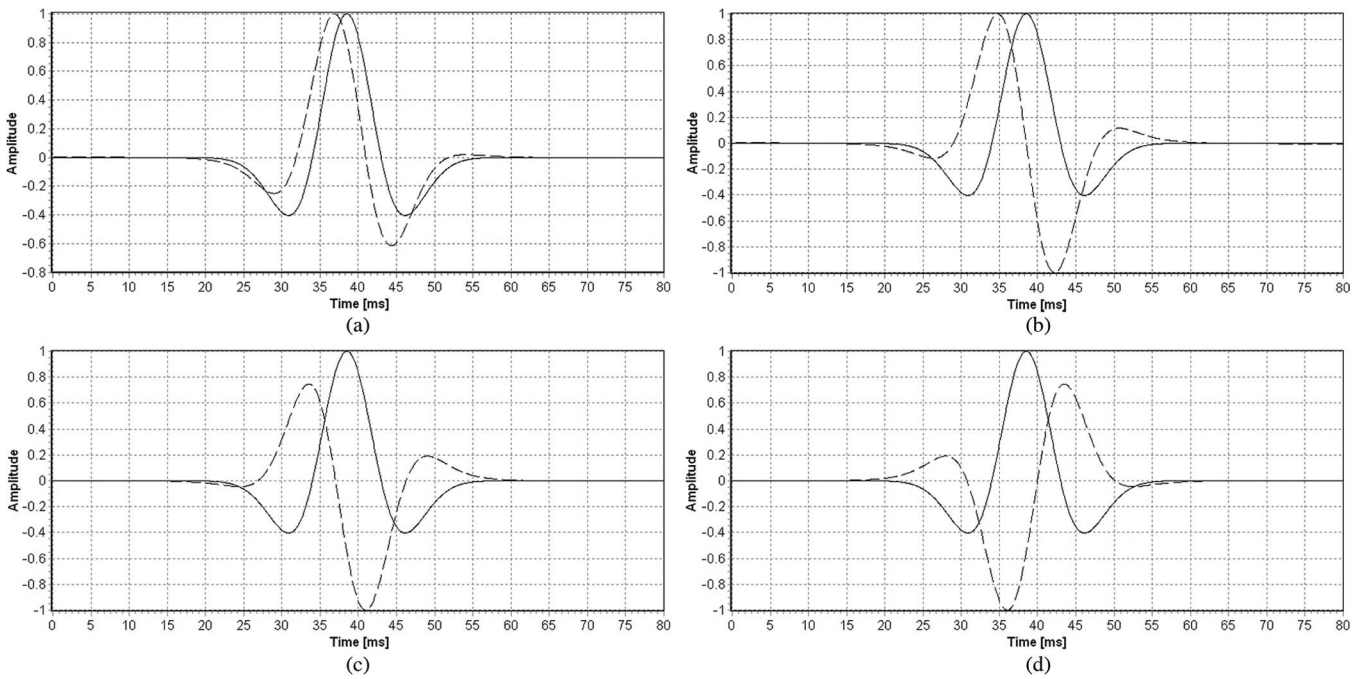

Fig. 5. (a) Ricker source wave -40° phase shift. (b) Ricker source wave -90° phase shift. (c) Ricker source wave -120° phase shift. (d) Ricker source wave -240° phase shift.

$v(t)$. The mathematical representation of this relationship is given as

$$z(t) = \int_0^t \mu(\tau) S(t-\tau) d\tau + \nu(t). \tag{9}$$

The discrete representation of (9) is given as

$$z(k) = \sum_{i=1}^{k} \mu(i) S(k-i) + \nu(k), \quad k = 1, 2, \ldots, N. \tag{10}$$

BSD has to be used when both $S(t)$ and $\mu(t)$ are unknown, but whenever the source wave is not stationary (as is the case when TIRs are present), simple BSD is not adequate. In that case, a more advanced version of this technique has to be applied, i.e., time-variant BSD (BSDtv).

C. PPD Algorithm

Baziw and Ulrych [19] and Baziw [20], [21] outlined a powerful BSD algorithm referred to as principle phase decomposition (PPD). In this algorithm, the source wave is uniquely modeled as an amplitude modulated sinusoid (AMS), which has been demonstrated to be a highly robust and accurate approximation for many analytical representations of seismic source waves (such as the exponentially decaying cyclic waveform, the mixed-phase Berlage wave, the zero-phase Ricker wave, and the zero-phase Klauder wave). In addition, the AMS wave has proven very accurate in modeling seismic data acquired during passive seismic monitoring [23]–[25] and vertical seismic profiling [21]. Fig. 6 illustrates the following three parameters that define the AMS source wave.

$\omega = 2\pi f$ the angular frequency, with f being the source wave's dominant frequency;

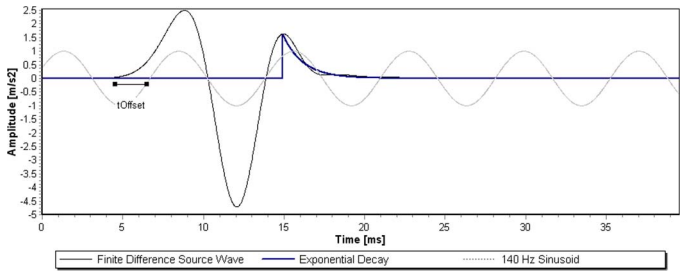

Fig. 6. Finite-difference source wave with superimposed 140-Hz sinusoid and exponential decay with a rate of 0.8/ms [21].

t_{offset} the offset time from the arrival time of the source wave, i.e., t_0, when the sinusoidal component commences;

h the exponential decay rate of the source wave.

In general terms, the AMS source wave is defined to be a sinusoid with a dominant frequency and phase modulated by an amplitude modulating term (AMT). The discrete representation of the AMS source wave is given as

$$\text{AMS}_k = \text{AMT}_k \sin[2\pi f_d \Delta k + \varphi] \tag{11}$$

where k denotes the time index, f_d denotes the dominant frequency, Δ denotes the sampling rate, and φ denotes the phase of the AMS source wave. Baziw [20] outlined how the phase of the source wave is readily determined from the arrival time $t_0' = t_0 + t_{\text{offset}}$ and the dominant frequency.

The most robust and best performing variant of the PPD algorithm is that which incorporates IFM (PPD-IFM). In general terms, this algorithm models the source wave as an AMS, and the overlapping source waves are treated as known inputs within a Kalman filter (KF) formulation based upon the current source wave and reflection series IFM parameter estimates.

The source wave and reflection series parameters are then obtained by iteratively minimizing a cost function defined to be the weighted RMS difference (RMSD) between the measured seismogram and the synthesized seismogram within the IFM algorithm. Baziw [21] described in detail the mathematical foundation and structure of the PPD-IFM algorithm, which provides very accurate estimations of the source wave and the corresponding reflection coefficients when processing noisy seismograms with stationary reflected source waves.

III. BSDSolver-tv Algorithm Outline

When the source wave is not stationary (as is the case with TIRs), the PPD-IFM algorithm has to be reformulated. As in the case with all optimal estimation solutions, the more *a priori* knowledge is specified, the more accurate the estimate results are. In this case, the following *a priori* information for TIRs can be incorporated in BSDtv.

- Although the phase of the source wave changes for each reflection, the dominant frequency remains the same [as previously outlined by (3) and (6)].
- The time width of the source wave remains constant.
- The reflected source waves are modeled as AMSs.
- The AMTs of the direct and reflected source waves remain constant.

In addition, the following *a priori* information from the BSD case also applies to BSDtv.

- The reflection coefficients are defined to be a scaled version of the maximum amplitude of the estimated source wave and are defined to reside within the bounds $0 \leq R \leq 1$.
- The reflection coefficients $R_0, R_1, R_2, R_3, \ldots, R_N$ must subsequently arrive later within the time series (i.e., $t_1 < t_2 < t_3, \ldots, t_N$) based upon the physics of reflection seismology.
- There is a minimum time separation between the reflection coefficients.
- There should not be a widely fluctuating AMT.
- Based upon experience, the AMT maximum, i.e., $\text{AMT}_{\max}$, resides within $1.3T$ of the onset of the source wave. Parameter T denotes the corresponding period of the dominant frequency of the source wave.
- A new AMT peak should not occur after $\text{AMT}_{\max}$.
- At time $T_{\max}$ from the arrival time t_0 of the source wave, we would expect that the AMT amplitude should have significantly decayed from $\text{AMT}_{\max}$ (i.e., $<5\%$). Parameter $T_{\max}$ denotes the maximum possible length of the source wave; it is an approximate variable and typically does not exceed $2.5T$.
- There are minimum and maximum bounds on the decay of the source wave, as outlined by Baziw [21].

Just as with the standard BSD algorithm, the BSDtv algorithm processes two to three seismic traces simultaneously utilizing dual- and quad-core central processing unit technology. When analyzing DST data, three adjacent depth traces within the vertical profile (e.g., traces recorded at depths 7, 8, and 9 m) are simultaneously processed, given the fact that there will be minimal variation between the first-arriving source waves recorded at adjacent depths.

TABLE I
SKFGEs for Known Inputs

Description	Mathematical Representation	Eq.
System equation.	$x_k = F_{k-1}x_{k-1} + \Lambda_{k-1}u_{k-1}$	12
Measurement equation	$z_k = H_k x_k$	13
State estimate extrapolation	$\hat{x}_{k\|k-1} = F_{k-1}\hat{x}_{k-1\|k-1} + \Lambda_{k-1}u_{k-1}$	14
Measurement extrapolation	$\hat{z}_k = H_k \hat{x}_{k\|k-1}$	15
Innovation	$\mathrm{I}_k = z_k - \hat{z}_k$	16
State estimate update	$\hat{x}_{k\|k} = \hat{x}_{k\|k-1} + \mathrm{I}_k / H_k$	17

x_k is the state (AMT) to be estimated, F_{k-1} the state transition matrix which describes the system dynamics, u_{k-1} a known deterministic time-varying input, Λ_{k-1} the relationship between x_k and u_{k-1}, and H_k the relationship between the state and the available measurement (seismogram)

The algorithm estimates the first-arriving source waves and reflection coefficients for the seismograms under analysis, where the weighted RMS error difference between the measured seismograms and the synthesized seismograms is minimized. The weight is defined as the absolute sum difference between the source wave parameters (i.e., ω, time location of the maximum peak $t_{\max}$, and the time duration of the estimated source wave for the seismic traces under analysis). The major difference between the BSD and BSDtv algorithms is that, in the former, the AMS (i.e., source wave) is assumed to be constant, whereas in the latter, the AMT component of the source wave is assumed to be constant.

Reference [21, Tables I and II] has been updated in this paper for the BSDtv algorithm. As described by Baziw [21], Table I outlines the KF governing equations for a known input. It is assumed that there is very low measurement noise and process noise (i.e., $\boldsymbol{Q}_k \to 0$ and $\boldsymbol{R}_k \to 0$) within the algorithm by preprocessing the data (i.e., digital, zero phase shift low- or bandpass frequency filter applied [26]) prior to inputting the seismogram into the BSDtv algorithm. For a single state estimation problem [only estimating the AMT component of the AMS source wave (AMT0)], the KF governing equations are then simplified, as outlined in Table I. In general terms, (14) and (15) are used to predict the state and the measurement, respectively; the innovation (16) is then calculated (difference between the actual and the predicted measurements); and the state is updated (17) by adding the predicted value (14) with the weighted innovation I_k/H_k.

Table II outlines the updated KF portion of the BSDtv algorithm for the case where it is assumed that there is a maximum of four reflected source waves overlapping the direct wave. The significant changes in the algorithm for BSD and that for BSDtv occur in Steps 2–4. First, while the BSD algorithm estimates the overlapping source waves as scaled (e.g., R_1) and time-shifted (e.g., $t - t_1$) versions of the direct source wave (e.g., $\text{SW1}(t) = R_1 \times \text{SW0}(t - t_1)$, the BSDtv algorithm estimates the AMT component of the overlapping source waves as scaled (e.g., R_1) and time-shifted (e.g., $t - t_1^*$) versions of the direct source wave AMT0 (e.g., $\text{AMT1}(t) = R_1 \times \text{AMT0}(t - t_1^*)$ and $\text{SW1}(t) = \text{AMT1}(t) \times \text{sin}_{\text{SW0}}(t - t_1)$, where $\text{sin}_{\text{SW0}}(t) = \sin[2\pi f_d(t) + \varphi_0]$). Then, there is also

TABLE II
BSDSOLVER-TV ALGORITHM FORMULATION

	Description	Mathematical Representation
1	Input parameters from IFM: ω, t_{Offset} (note: the sinusoidal arrival time is defined as $t_0' = t_0 + t_{offset}$), h, R_0, R_1, R_2, R_3, R_4, t_1, t_2, t_3 and t_4.	The five possible overlapping source waves are denoted as $SW0_k$, $SW1_k$, $SW2_k$, $SW3_k$, & $SW4_k$. Set parameter AMT_EXP = FALSE Process time series from time (*note* : $t = \Delta k$) $t = t_0$ to $t = t_0 + T_{\max}$ ($T_{\max}$ denotes the maximum possible length of the source wave)
	Initialize source waves (*SWN*) and *AMTs* for time index *k=0*.	$SW0_k = SW1_k = SW2_k = SW3_k = SW4_k = 0$ N = source wave index (N = *0, 1, 2, 3, 4*).
2	If $t < t_1$ then utilize single KF equations outlined in Table I to obtain a new estimate of the direct source wave AMT (*AMT0*).	$AMT\ 0_{k\|k} = AMT\ 0_{k-1\|k-1} + I_k / H_k$ If $t < t_0'$ then $H_k = R_0$ If $t \geq t_0'$ then $H_k = R_0 \times \sin[\,2\pi f t + \varphi_0\,]$ or $1/H_k = \text{cosecant}\ [2\pi f t + \varphi_0]/R_0$ note: $AMT\ 0_{k\|k-1} = AMT\ 0_{k-1\|k-1}$ and $R_0 = 1$
3	If $t \geq t_1$ then Implement SKFGE eqs. (18a) to (18f), (19a) and (19b). Calculate Innovation utilizing (19a), (19b), and (16).	For the direct and overlapping source waves (*N = 0, 1, 2, 3, 4*) update $AMTN_k$ and SWN_k If $AMTN_{k\|k-1} \leq 0.01 \times R_N$ apply (20). If $AMTN_{k\|k-1} > 0.01 \times R_N$ apply (21). If AMT_EXP = TRUE then $AMT\ 0_k = AMT\ 0_{k-1} \times \exp^{-h(t-t\exp)}$ note: $AMTN_{k\|k-1} = AMTN_{k-1\|k-1}$
4	In the BSDSolver-tv™ the maximum of the AMT0 or source wave is assumed to occur within time 1.3T (*T=1/f*).	Track AMT0 maximum (AMT_{MAX}). If the AMT0 maximum exceeds 1.3T then there is an early exit from the KF with an error flag.
5	When the AMT0 value drops below 0.6 $\times AMT_{MAX}$ at time index t_{exp}, then apply exponential decay estimate. AMT_EXP = TRUE	$AMT\ 0_k = AMT\ 0_{k-1} \times \exp^{-h(t-t\exp)}$
6	Based upon new $AMTN_{k\|k}$ update SWN_k. $SWN_k = AMTN_k \times HN_k$	
7	Let k = k+1 & iterate to step 2.	
8	Calculate RMS error residual and return value to IFM algorithm.	$E = \sum_{k=k_0}^{k_0+k_1} \left[z_k - \begin{pmatrix} SW\,0_k + SW1_k + SW\,2_k \\ + SW\,3_k + SW\,4_k \end{pmatrix} \right]$ $E_{RMS} = \sqrt{E/k_1}$ note: $k_0 = t_0/\Delta$ & $k_1 = T_{\max}/\Delta$

an important distinction between time index t_N, which denotes the IFM start time of the sinusoidal component of the AMS overlapping source wave. In the case of BSD, this parameter was defined as the reflection series arrival time input (i.e., arrival time of overlapping or reflected source wave at index N) for a specific iteration of the downhole simplex technique [21], but for BSDtv, the AMS sinusoidal component of the overlapping or the reflected source is time shifted by t_N.

Finally, time index t_N^* is introduced in the BSDtv algorithm, and it denotes the case when the KF estimated AMT of the reflected source wave exceeds 1% of the IFM inputted reflection coefficient (e.g., $0.01 \times R_N$). At this time index, the AMT of the reflected source wave is calculated as scaled and time-shifted versions of the direct source AMT (e.g., $\text{AMTN}(t) = R_N \times \text{AMT0}(t - t_N^*)$). The incorporation of two time indices for each reflected source wave allows for variable phase sinusoids within the constant AMT0 envelope, which is required for TIRs.

When deriving the reflected source wave KF AMT estimation equations as outlined in Step 2 in Table II, it is again assumed that there is very low measurement noise and process noise (i.e., $\boldsymbol{Q}_k \to 0$ and $\boldsymbol{R}_k \to 0$). In addition, it is also assumed that the error covariance between the AMTs of the reflected source waves is zero (i.e., the AMTs are independent). These assumptions allow for significantly simplified KF governing equations when determining the time index when $\text{AMTN}(t)$ exceeds $0.01 \times R_N$, and the BSDtv algorithm has been shown to perform very well with these simplifications.

The governing equations (Step 3 in Table II) for estimating the AMTs of the reflected source waves AMTN using the simplified KF governing equations (SKFGEs) are as follows:

$$H0_k = R_0 \times \sin\left[2\pi f_d(k\Delta) + \varphi_0\right] \tag{18a}$$
$$H1_k = R_1 \times \text{sin}_{\text{SW0}}(\Delta_1) \tag{18b}$$
$$H2_k = R_2 \times \text{sin}_{\text{SW0}}(\Delta_2) \tag{18c}$$
$$H3_k = R_3 \times \text{sin}_{\text{SW0}}(\Delta_3) \tag{18d}$$
$$H4_k = R_4 \times \text{sin}_{\text{SW0}}(\Delta_4) \tag{18e}$$
$$D_k = H0_k^2 + H1_k^2 + H2_k^2 + H3_k^2 + H4_k^2 \tag{18f}$$

where Δ is the sampling rate, $t = \Delta \times k$, $\Delta_N = (t - t_N)$, $R_0 = 1.0$ (direct source has maximum amplitude), and $\text{sin}_{\text{SW0}}(\Delta_N) = \sin[2\pi f_d(\Delta_N) + \varphi_0]$. Measurement extrapolation is as follows:

$$\hat{z}_k = \text{SW0}_k + \text{SW1}_k + \text{SW2}_k + \text{SW3}_k + \text{SW4}_k \tag{19a}$$
$$\text{SWN}_k = \text{AMTN}_k \times HN_k. \tag{19b}$$

Innovation is as follows:

$$I_k = z_k - \hat{z}_k \tag{16}$$

AMTN estimate update for case $\text{AMTN}_{k|k-1} \leq 0.01 \times R_N$, i.e.,

$$\text{AMTN}_{k|k} = \text{AMTN}_{k|k-1} + [I_k \times HN_k / D_k]. \tag{20}$$

AMTN estimate update for case $\text{AMTN}_{k|k-1} > 0.01 \times R_N$; note that $t_N^* = t$, when $\text{AMTN}_{k|k} = 0.01 \times R_N$, i.e.,

$$\text{AMTN}(t) = R_N \times \text{AMT0}\,(t - t_N^*)\,. \tag{21}$$

In the current formulation of the BSDtv algorithm, there are two stages of analysis identical to those of the first two stages of the BSD algorithm [21], albeit in the BSDtv case, a sampling rate of 90 samples/T is specified. In the second stage of the BSDtv algorithm, the IFM technique is implemented, and the top source wave estimates are determined, where the

weighted RMSD between the estimated seismograms and the true seismograms over time window t_0 (source wave arrival time) to $t_0 + T_{\max}$ ($T_{\max}$ denotes the maximum possible length of the source wave) is minimized. It should be noted that, in the BSD algorithm, there are three stages of analysis to allow for interpolation of the SW0 or the AMT0 data points. This AMT0 data interpolation is not yet implemented in the current version of the BSDtv algorithm when $\text{AMTN}_{k|k-1} \leq 0.01 \times R_N$.

As previously outlined, the weight [see (23)] of the cost function is defined as the RMSD between the source wave parameters of dominant frequency f, $t_{\max}$ [the time location of $\text{AMT}_{\max}$ (the maximum value of the AMT)], and t_{width} (the time duration of the estimated source wave)]. The weight calculation is then as in (22a)–(23), shown at the bottom of the page, where $f_{\text{mean}} = (f_1 + f_2 + f_3)/3$, $t_{\text{meanMax}} = (t_{\max 1} + t_{\max 2} + t_{\max 3})/3$, and $t_{\text{width}} = (t_{\text{width1}} + t_{\text{width2}} + t_{\text{width3}})/3$.

The subscripts (1, 2, and 3) in (22a)–(22c) denote the independent seismic traces simultaneously under analysis. As previously outlined, when analyzing DST data, three adjacent depth traces within the vertical profile are simultaneously processed, given the fact that there will be minimal variation between the first-arriving source waves recorded at adjacent depths.

IV. BSDSolver-tv Simulation Results

The implementation and performance of the BSDSolver-tv algorithm is demonstrated by considering the analysis of three DST challenging synthetic seismograms. The seismograms were outlined by Baziw and Verbeek [10] and represent a simulated vertical seismic profile (VSP). The simulated data sets are challenging due to the fact that the direct and reflected source waves are time variant and there are five closely spaced equivalent reflection coefficients with dipoles, but this allows for a better assessment of the performance and capabilities of the BSDSolver-tv algorithm then when relatively simplistic seismograms are used.

Fig. 4 outlines a 2-D SH source wave SCPT investigation where we have stone columns of diameter $R = 1.0$ m. Insertions of stone columns are a ground improvement technique to increase the load-bearing capacity of the soil. Fig. 7 shows distributions of estimated shear and compression wave velocities for sites distributed throughout Japan [22]. In this figure, the velocity estimates are arranged by age (alluvial, diluvial, and tertiary ground) and soil type. Referring to the typical S-wave velocities outlined in Fig. 7, the SH-wave SCPT simulation test is carried out in a fairly homogeneous alluvial sand with S-wave velocities varying from 180 to 240 m/s. From the surface down to a depth of 5 m, we have a homogeneous SH-wave velocity of 180 m/s. Between depths 5 and 6 m, the *in situ* SH-wave

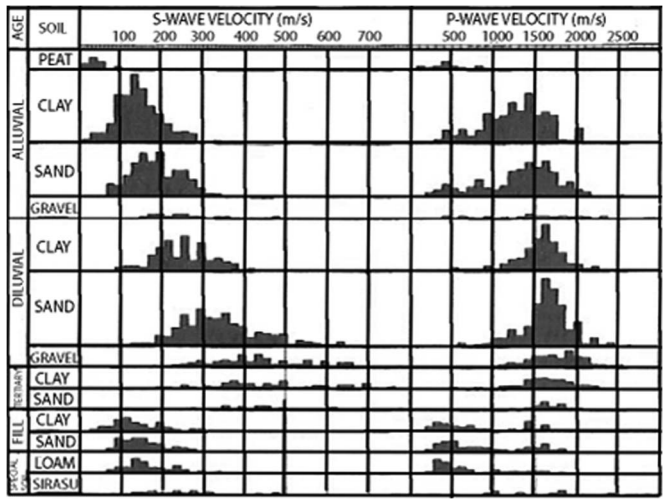

Fig. 7. Distributions of P- and S-wave velocities [22].

velocity is 240 m/s, and between depths 6 and 7 m, the SH-wave velocity is 196 m/s. Fig. 4 illustrates five source ray paths. Ray path 2 is the direct wave, whereas ray paths 1, 3, 4, and 5 are the reflected waves. For this VSP simulation, a source-sensor radial offset (parameter l_2 in Fig. 4) of 1.5 m was assumed; therefore, referring to Fig. 2, the slant distances, i.e., d_i, for the simulation depths of 5, 6, and 7 m are 5.22, 6.18, and 7.16 m, respectively. We are interested in the interval velocities between depths 5 and 6 m and depths 6 and 7 m. Due to the constructive/destructive interference of the reflected source waves, it is not possible to utilize time markers (e.g., 2, C, 3, and D in Fig. 1) or the cross-correlation function or the cross-power spectrum in obtaining relative arrival times ΔT; therefore, it is necessary to apply a BSDtv technique so that the direct source wave is extracted from the recorded seismogram and relative arrival times can be readily obtained.

In order to have challenging and realistic seismogram simulations, the time offset between overlapping source waves is set to vary from 3 to 5 ms. For example, in Fig. 4, the travel path for source wave 1 is defined as $SD = SD1 + SD2$, and the known parameters are H (probe depth $H = H_1 + H_2$), l_1, and l_2 (note: $l = l_1 + l_2$). Utilizing the following trigonometric relationship, the travel distances and the travel time for reflected source wave 1 can be determined.

Trigonometric relationships (see Fig. 4) are as follows:

$$H_1 = \frac{l}{\tan \beta_1} \tag{24}$$

$$H_2 = \frac{l_1}{\tan \beta_1} \tag{25}$$

$$W_f = \sqrt{\left((f_1 - f_{\text{mean}})^2 + (f_2 - f_{\text{mean}})^2 + (f_3 - f_{\text{mean}})^2\right)/3} \tag{22a}$$

$$W_{t\max} = \sqrt{\left((t_{\max 1} - t_{\text{meanMax}})^2 + (t_{\max 2} - t_{\text{meanMax}})^2 + (t_{\max 3} - t_{\text{meanMax}})^2\right)/3} \tag{22b}$$

$$W_{t\text{width}} = \sqrt{\left((t_{\text{width1}} - t_{W\text{mean}})^2 + (t_{\text{width2}} - t_{W\text{mean}})^2 + (t_{\text{width3}} - t_{W\text{mean}})^2\right)/3} \tag{22c}$$

$$\text{Weight} = \lfloor W_f + W_{t\max} + W_{t\text{width}} \rfloor / 3 \tag{23}$$

$$\theta_1 = 90^\circ - \beta_1 \tag{26}$$

$$\beta_1 = \tan^{-1}\left((l + l_1)/H\right) \tag{27}$$

$$SD1 = \sqrt{H_1^2 + l^2} \tag{28}$$

$$SD2 = \sqrt{H_2^2 + l_1^2} \tag{29}$$

Travel Distance for Source Wave 1:

$$SD = SD1 + SD2 \tag{30}$$

Travel Time for Source Wave 1:

$$t = SD/V. \tag{31}$$

Substituting $l_1 = 1$ m, $l_2 = 1.5$ m ($: l = l_1 + l_2 = 2.5$ m), and $H = 5$ m into (27) gives $\beta_1 = 35^\circ$; therefore, $H_1 = 3.57$ m, and $H_2 = 1.43$ m. Substituting these values into (28)–(30) gives a travel distance of 6.11 m. This results in a travel distance difference between direct wave 2 and reflected wave 1 of 0.89 m (i.e., 6.11–5.22). Utilizing $V = 180$ m/s and (31) results in a 4.94-ms arrival time difference; therefore, the 3- to 5-ms time offset between overlapping source waves would appear to be reasonable.

In this DST data set, Berlage source waves were generated and superimposed at depths of 5, 6, and 7 m. These waves are defined as [10], [19]–[21]

$$\omega(t) = AH(t)t^n e^{-ht}\cos(2\pi f t + \theta) \tag{32}$$

where $H(t)$ is the Heaviside unit step function ($H(t) = 0$ for $t \leq 0$, and $H(t) = 1$ for $t > 0$). The amplitude modulation component is controlled by two factors: the exponential decay term h and the time exponent n. These parameters are considered to be nonnegative real constants. All simulated waves had the common values of $f = 70$ Hz, $n = 2$, and $h = 270$ specified. The phase values were set at $\phi = 20^\circ, 40^\circ, 140^\circ$, and 250°, respectively. The arrival times[3] and maximum amplitudes were set as follows for the five Berlage source waves:

- at a depth of 5 m: (5 ms, 1), (8 ms, 0.75), (11 ms, 0.625), (17 ms, 0.8), and (22 ms, 0.65), respectively (see Figs. 8 and 9);
- at a depth of 6 m: (9 ms, 1), (14 ms, 0.75), (17 ms, 0.625), (21 ms, 0.8), and (24 ms, 0.65), respectively (see Figs. 10 and 11);
- at a depth of 7 m: (14 ms, 1), (17 ms, 0.75), (21 ms, 0.625), (24 ms, 0.8), and (29 ms, 0.65), respectively (see Figs. 12 and 13).

Each depth superposition of the source waves is shown with the reflection coefficients to allow for the visualization of the arrival time and maximum amplitude values [Fig. 9—"Seismogram 1" (S1); Fig. 11—"Seismogram 2" (S2); Fig. 13—"Seismogram 3" (S3); for the depths of 5, 6, and 7 m, respectively].

[3]The first 24 ms of data of seismograms 1, 2, and 3 have been removed due to the fact that no seismic data are contained within the first 24 ms, and we are only interested in relative arrival times between depths 5 and 6 m and 6 and 7 m.

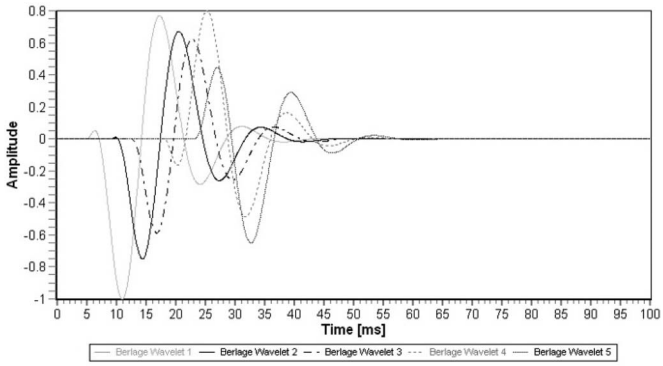

Fig. 8. Simulation 1—Berlage source waves with varying phases [10].

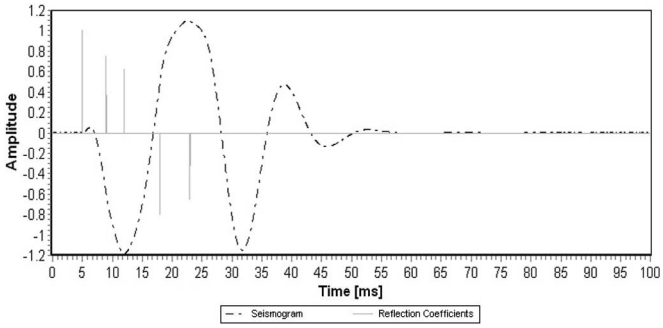

Fig. 9. Superposition of Berlage source waves illustrated in Fig. 8 [10].

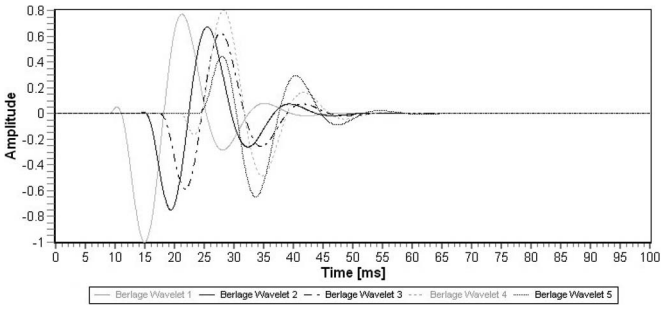

Fig. 10. Simulation 2—Berlage source waves with varying phases [10].

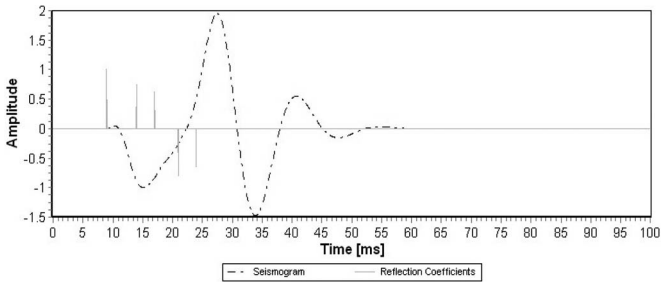

Fig. 11. Superposition of Berlage source waves illustrated in Fig. 10 [10].

As previously stated, we are interested in the interval velocities and the associated relative arrival times between depths 5 and 6 m and depths 6 and 7 m. For slant distances of 5.22, 6.18, and 7.16 m and assuming a straight ray travel path (i.e., no refraction), the first-arriving direct source wave interval velocities can be calculated as $V_{5-6} = (6.18 - 5.22)/(9 - 5) = 240$ m/s for depth interval 5–6 m and $V_{6-7} = (7.16 - 6.18)/(14 - 9) = 196$ m/s for depth interval 6–7 m.

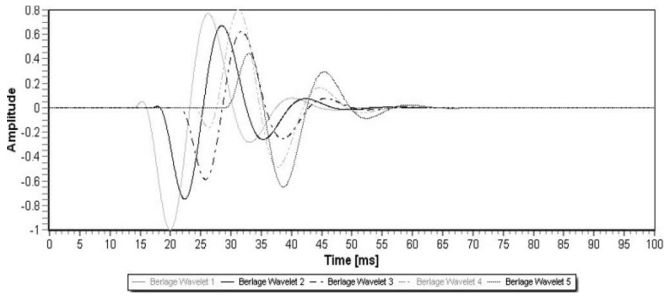

Fig. 12. Simulation 3—Berlage source waves with varying phases [10].

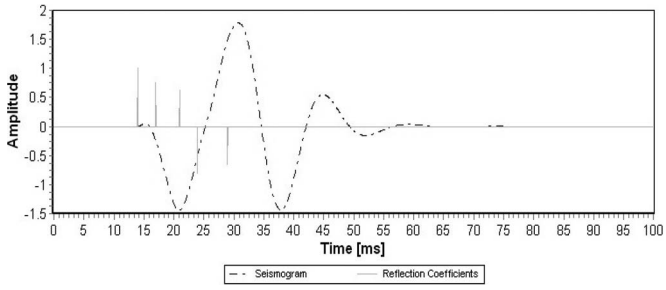

Fig. 13. Superposition of Berlage source waves illustrated in Fig. 12 [10].

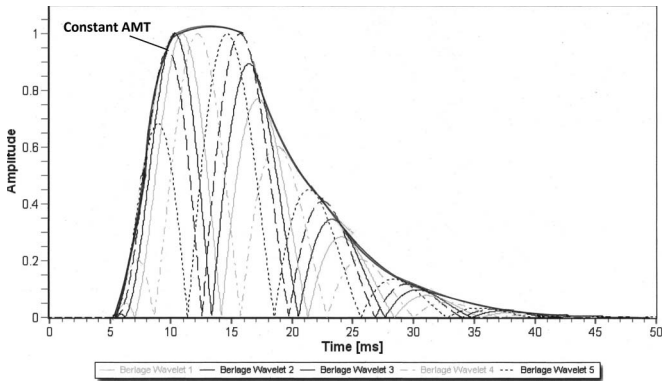

Fig. 14. Constant AMT for the Berlage source waves shown in Fig. 8. Berlage Wavelets 1–5 have the same 5-ms arrival time specified so that the constant AMT can be demonstrated.

Fig. 14 illustrates the concept of a constant AMT for TIRs. In this figure, the absolute amplitudes of the source waves outlined in Fig. 8 are superimposed with an identical arrival time of 5 ms specified for each wave. The dark AMT outline shown in Fig. 14 illustrates that all TIRs can be modeled as AMSs where there is a constant AMT envelop. This is why the AMT component of the direct and reflected source waves is assumed constant in the BSDSolver-tv algorithm.

In the first test, the seismograms outlined in Figs. 9, 11, and 13, were processed on a "stand-alone" basis. This test bed analysis was carried out in order to obtain an initial assessment on the ability of the BSDSolver-tv algorithm to carry out BSDtv when the RMSD weight outlined in (23) is not implemented and *a priori* knowledge of the source wave dominant frequency is available. For example, the trough at the end of the seismogram shown in Fig. 9 has an approximate duration of 7 ms (i.e., 43–50 ms). This represents a duration of $T/2$, where T is the period of the source wave; therefore, $T/2 = 7$ ms, which implies that $T = 14$ ms, which gives an approximate dominant frequency of $f_d = 1/T = 71$ Hz. In the stand-alone

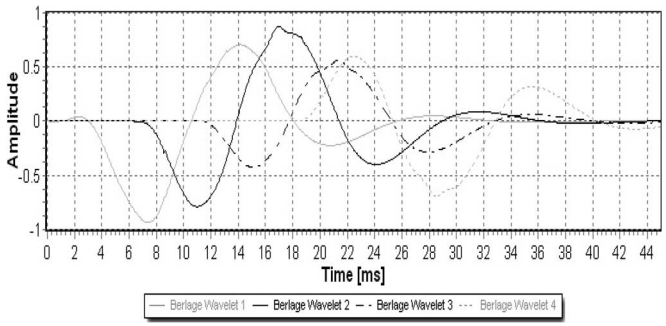

Fig. 15. BSDSolver-tv estimated source waves for the seismogram illustrated in Fig. 9 (S1).

analysis, the dominant frequency window is set from 68 to 71 Hz. In addition, the simulated seismograms were fed into the BSDSolver-tv algorithm without skipping data points (i.e., reduce computation time by "coarsening" sampling). The sampling rate of the simulated seismograms is 0.05 ms. Additional parameters set were a minimum and a maximum source wave length of $1.2T$ and $2.5T$, respectively.

The preprocessing steps of the BSDSolver-tv algorithm are outlined as follows.

- Normalize the seismograms under analysis.
- Starting at the beginning of the normalized seismogram, identify the time index, i.e., $\acute{t}$, when the absolute value of the amplitude exceeds 0.07.
- Move back in time from $\acute{t}$ until the first zero-crossing is reached and identify this time index as t_0.
- Move back in time from t_0 by 3 ms and identify this start time as t_0'.
- Start data processing at time index t_0'. Data from $t = 0$ to $t = t_0'$ are ignored within the BSDSolver-tv algorithm to reduce processing time. This time span is padded back into the front end of the processed seismogram post implementation of BSDSolver-tv. For example, if $t_0 = 15$ m/s, the algorithm starts processing data at $t_0' = 12$ ms. After application of BSDSolver-tv, 12 ms of data are padded (with zeros) to the front end of the processed seismogram.

These preprocessing steps are implemented so that the required time length of the seismograms under analysis is minimized, which, in turn, minimizes the processing time. For example, in deeper DST investigations, source waves arrive much later in the recorded seismograms, and the early portion of the data contains no useful information; therefore, there is no need to process this portion of the seismogram. This preprocessing has no impact on the BSDSolver-tv estimated source waves. It only allows for reduction in processing time. After processing the inputted seismograms, the algorithm saves the estimated source waves corrected for their original start times and maximum amplitudes.

Fig. 15 shows the BSDSolver-tv estimated source waves for the seismogram illustrated in Fig. 9 (S1). The estimated Berlage wavelets shown in Fig. 15 have a dominant frequency of 66.7 Hz, which is 1.3 Hz below the lower limit of the algorithm frequency window since the IFM portion has a built-in margin of 2 Hz (i.e., the estimated values may range from 66 to 73 Hz). As illustrated in Fig. 15, the estimated source waves (Berlage

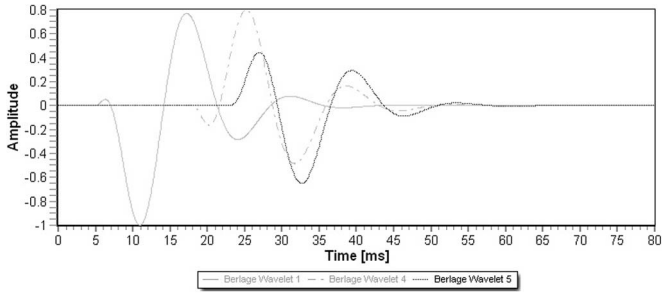

Fig. 16. Seismogram S1 overlapping source waves Berlage Wavelets 1, 4, and 5.

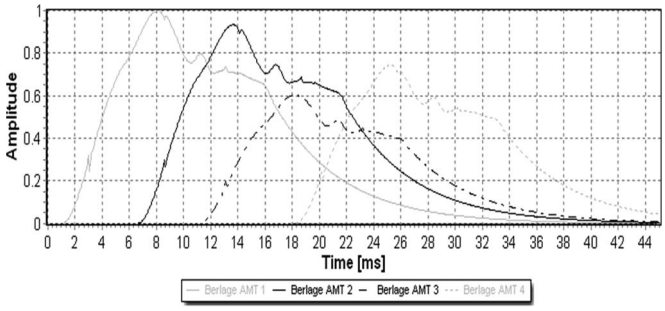

Fig. 17. BSDSolver-tv estimated AMT components for the seismogram illustrated in Fig. 9 (S1).

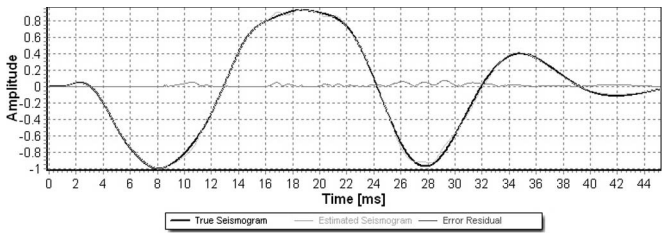

Fig. 18. BSDSolver-tv estimated seismogram, true seismogram, and corresponding residual error (S1).

Wavelets 2, 3, and 4) have very comparable arrival times to the true values shown in Fig. 8, when adding 4 ms to the arrivals shown in Fig. 15 due to the preprocessing described above, as shown in the following:

- Wavelet 2—first trough: 14.8 ms estimated versus 14.3 ms actual;
- Wavelet 3—first trough: 18.7 ms estimated versus 17 ms actual;
- Wavelet 4—peak: 26.4 ms estimated versus 25.3 ms actual.

As shown in Fig. 15, a negligible Berlage Wavelet 5 was estimated. It is believed that this is due to the fact that Berlage Wavelets 1 and 4 "mask" Berlage Wavelet 5, as shown in Fig. 16. Fig. 17 illustrates the AMT components of the source waves shown in Fig. 15, whereas Fig. 18 shows the estimated normalized seismogram superimposed upon the true normalized seismogram with a corresponding RMS error of 0.0008 units. The BSDSolver-tv estimated and normalized Berlage Wavelet 1 is illustrated in Fig. 19 superimposed upon the true normalized source wave. The estimated Berlage Wavelet 1 (which will be used later to determine the interval velocities) is smoothed by applying a low-pass filter applied with a cutoff of 3^* dominant frequency (i.e., 66.7 Hz). As shown in Fig. 19,

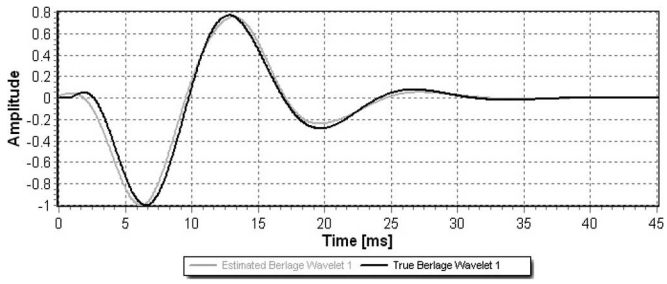

Fig. 19. BSDSolver-tv estimated Berlage Wavelet 1 superimposed upon the true Berlage Wavelet 1 (S1).

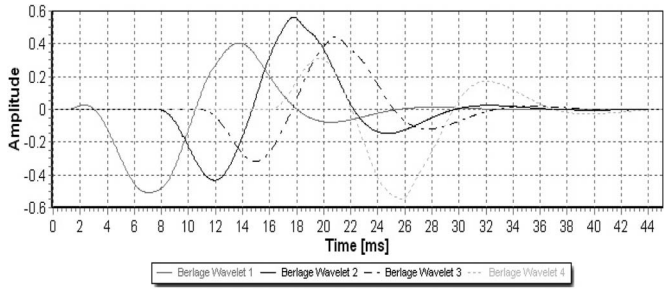

Fig. 20. BSDSolver-tv estimated source waves for the seismogram illustrated in Fig. 11 (S2).

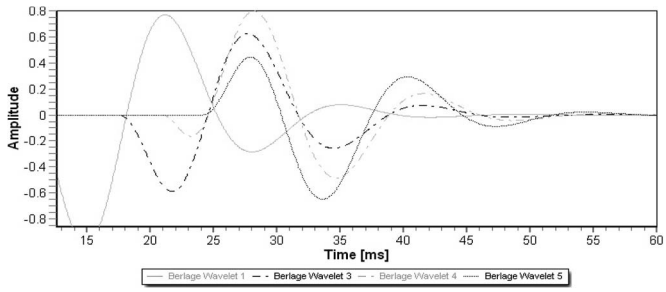

Fig. 21. Seismogram S2 overlapping source waves Berlage Wavelets 1, 3, 4, and 5.

there is very close agreement between the estimated and true Berlage Wavelet 1. Although the direct first-arriving source wave (Berlage Wavelet 1) is utilized to obtain *in situ* velocities, the estimated overlapping (reflected) source waves identify and quantify the vertical inclusions and bounding geological layers.

Fig. 20 shows the BSDSolver-tv estimated source waves for the seismogram illustrated in Fig. 11 (S2). The estimated Berlage wavelets outlined in Fig. 20 have a dominant frequency of 66.8 Hz. Once again, as illustrated in Fig. 20, the estimated source waves (Berlage Wavelets 2, 3 and 4) have generally very comparable arrival times to the true values shown in Fig. 13, when adding 6 ms to the arrivals shown in Fig. 20 due to the preprocessing described above, as shown in the following:

- Wavelet 2—first trough: 19 ms estimated versus 19.2 ms actual;
- Wavelet 3—first trough: 21 ms estimated versus 21.6 ms actual;
- Wavelet 4—first peak: 26 ms estimated versus 28 ms actual.

Similar to the previous case, a negligible Berlage Wavelet 5 was estimated. It is believed that this is again due to the fact that Berlage Wavelets 1, 3 and 4 mask Berlage Wavelet 5, as shown

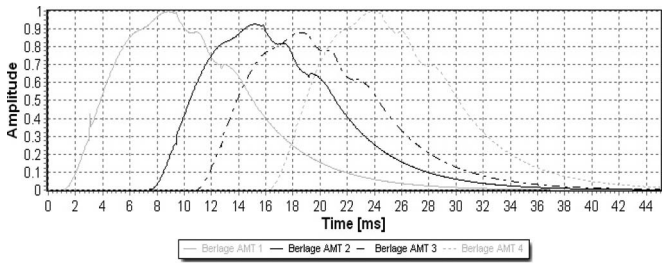

Fig. 22. BSDSolver-tv estimated AMT components for the seismogram illustrated in Fig. 11 (S2).

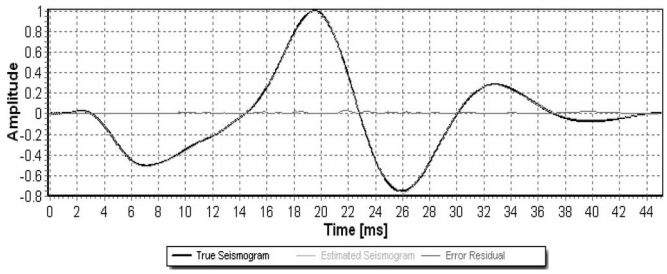

Fig. 23. BSDSolver-tv estimated seismogram, true seismogram, and corresponding residual error (S2).

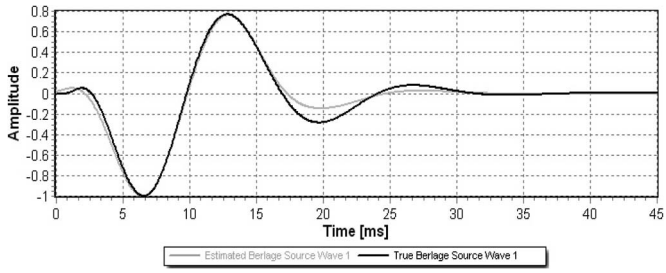

Fig. 24. BSDSolver-tv estimated Berlage Wavelet 1 superimposed upon the true Berlage Wavelet 1 (S2).

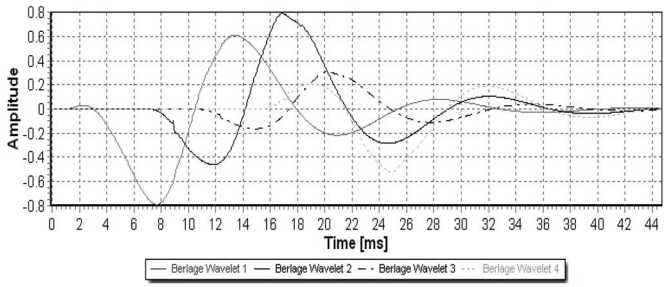

Fig. 25. BSDSolver-tv estimated source waves for the seismogram illustrated in Fig. 13 (S3).

in Fig. 21. Fig. 22 illustrates the AMT components of the source waves shown in Fig. 20, whereas Fig. 23 shows the estimated normalized seismogram superimposed upon the true normalized seismogram with a corresponding RMS error of 0.0004 units. The BSDSolver-tv estimated and normalized Berlage Wavelet 1 is illustrated in Fig. 24 superimposed upon the true normalized source wave. The estimated Berlage Wavelet 1 is smoothed by applying a low-pass filter applied with a cutoff of 3^* dominant frequency (i.e., 66.8 Hz). As shown in Fig. 24, there is very close agreement between the estimated and true Berlage Wavelet 1.

Fig. 25 shows the BSDSolver-tv estimated source waves for the seismogram illustrated in Fig. 13 (S3). The estimated

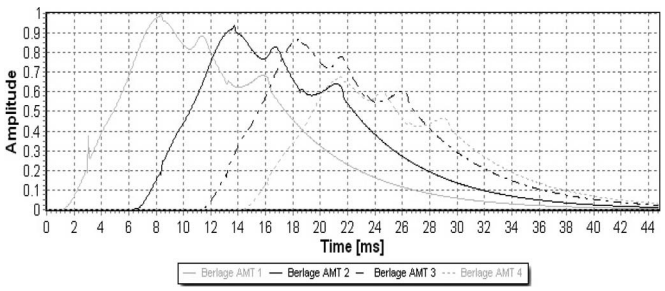

Fig. 26. BSDSolver-tv estimated AMT components for the seismogram illustrated in Fig. 13 (S3).

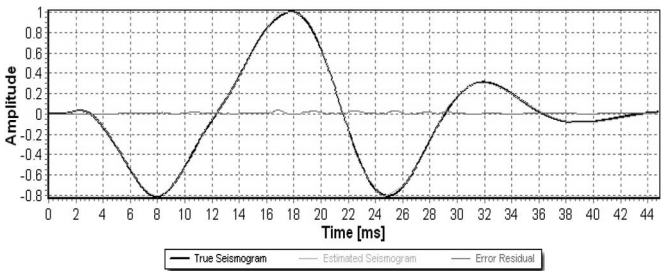

Fig. 27. BSDSolver-tv estimated seismogram, true seismogram, and corresponding residual error (S3).

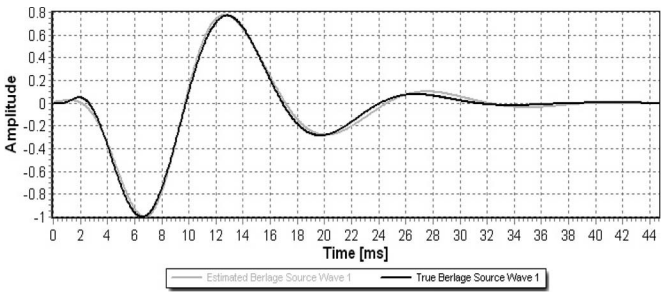

Fig. 28. BSDSolver-tv estimated Berlage Wavelet 1 superimposed upon the true Berlage Wavelet 1 (S3).

Berlage wavelets outlined in Fig. 25 have a dominant frequency of 67.1 Hz. Once more, as illustrated in Fig. 25, the estimated source waves (Berlage Wavelets 2, 3, and 4) have very comparable arrival times to the true values shown in Fig. 12, when adding 13 ms to the arrivals shown in Fig. 25 due to the preprocessing described above, as shown in the following:

- Wavelet 2—first trough: 24.5 ms estimated versus 22.5 ms actual
- Wavelet 3—first trough: 27.5 ms estimated versus 26.2 ms actual
- Wavelet 4—peak: 31 ms estimated versus 31.5 ms actual

As shown in Fig. 25, a negligible Berlage Wavelet 5 was estimated. It is again believed that this is due to the fact that Berlage Wavelet 4 masks Berlage Wavelet 5. Fig. 26 illustrates the AMT components of the source waves shown in Fig. 25, whereas Fig. 27 shows the estimated normalized seismogram superimposed upon the true normalized seismogram with a corresponding RMS error of 0.0004 units. The BSDSolver-tv estimated and normalized Berlage Wavelet 1 is illustrated in Fig. 28 superimposed upon the true normalized source wave. The estimated Berlage Wavelet 1 is smoothed by applying a low-pass filter applied with a cutoff of 3^* dominant frequency

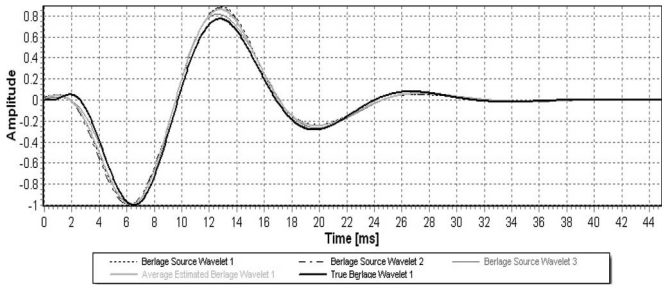

Fig. 29. BSDSolver-tv estimated Berlage Wavelet 1 for seismograms S1, S2, and S3 and the corresponding averaged seismogram superimposed upon the true Berlage Wavelet 1.

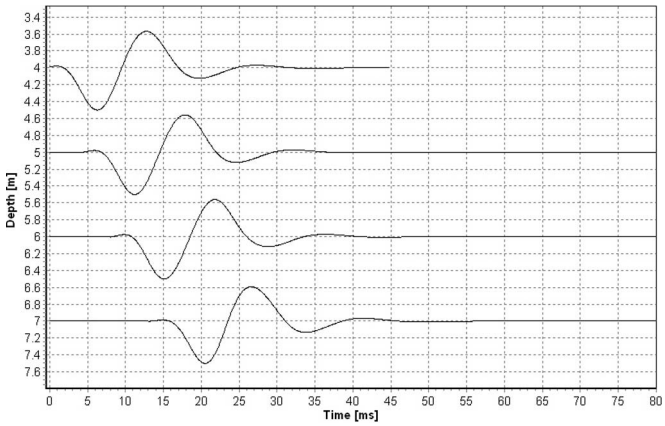

Fig. 30. VSP of estimated Berlage wavelets shown in Fig. 29. The seismic trace displayed at 4 m is the averaged Berlage Wavelet 1 illustrated in Fig. 29.

(i.e., 67.1 Hz). As shown in Fig. 28, there is very close agreement between the estimated and true Berlage Wavelet 1.

In the second test, the seismograms S1, S2, and S3 were simultaneously processed with a coarsening sampling rate of 90 samples/T or 0.15 ms. As previously outlined, in the second stage of the algorithm, the IFM technique is implemented, and the top source wave estimates are determined, where the weighted RMSD between the estimated and true seismograms are minimized. The weight of the cost function was given by (23). In this test case, the dominant frequency window is set from 63 to 83 Hz. The dominant frequency window has been increased to test the case when then there is limited prior knowledge on the source wave dominant frequency and BSDSolver-tv is required to estimate this value within a larger window. The increase in the frequency window can be justified since a weighted RMSD is applied.

Fig. 29 illustrates the estimated Berlage Wavelet 1 for seismograms S1, S2, and S3 and the corresponding averaged seismogram superimposed upon the true Berlage Wavelet 1, which shows that there is very close agreement between the estimated, averaged, and true Berlage Wavelet 1. Fig. 30 illustrates the time-corrected (i.e., preprocessing data windowing removed) VSP of the estimated Berlage Wavelet 1 for each seismogram shown in Fig. 29. In Fig. 30, the seismic trace displayed at 4 m is the averaged Berlage Wavelet 1 illustrated in Fig. 29. For the standard BSD case, this estimated averaged source wave could be utilized within the water level technique [20], [21] to obtain estimates of the associated reflection coefficients.

These traces were then subjected to the cross-correlation technique (CCT) [6], which is a standard methodology to obtain DST interval velocities. The CCT is based upon cross correlating the waves recorded at consecutive depth increments, whereby the value of the time shift at the maximum cross-correlation value is assumed to be the relative travel time difference for the wave to travel the depth increment. Cross correlating the estimated Berlage Wavelet 1 for seismograms S1, S2, and S3 results in the relative arrival times of 3.95 ms (true value $= 4$ ms) and 5.08 ms (true value $= 5$ ms) for depth increments 5–6 m and 6–7 m, respectively. The corresponding interval velocities assuming a straight ray travel path are calculated as $V_{5-6} = (6.18 - 5.22)/(3.95) = 240$ m/s for depth interval 5–6 m and $V_{6-7} = (7.16 - 6.18)/(5.1) = 192$ m/s for depth interval 6–7 m. This compares very close to the true values of $V_{5-6} = 241$ m/s and $V_{6-7} = 196$ m/s.

It should be noted that, as outlined by Baziw and Verbeek [10], it is not possible to accurately obtain relative arrival times utilizing time markers or the CCT when processing undeconvolved seismograms containing TIRs. For example, cross correlating seismograms S1, S2, and S3 results in the relative arrival times of 3.1 ms (true value $= 4$ ms) and 3.8 ms (true value $= 5$ ms) for depth increments 5–6 m and 6–7 m, respectively. The corresponding interval velocities assuming a straight ray travel path are calculated as $V_{5-6} = (6.18 - 5.22)/(3.15) = 305$ m/s for depth interval 5–6 m and $V_{6-7} = (7.16 - 6.18)/(3.8) = 258$ m/s for depth interval 6–7 m. These estimated values have corresponding percent errors of 27% and 32%, respectively.

V. Conclusion

Accurate *in situ* P- and S-wave velocity profiles are essential in geotechnical foundation designs. These parameters are used in both static and dynamic soil analyses where the elastic constants are input variables into the models defining the different states of deformations. The DST and the CST are geotechnical *in situ* site characterization tools, which enable direct V_S and V_P *in situ* velocities to be accurately estimated. In DST and CST, the *in situ* V_S and V_P velocities are determined by obtaining the corresponding source wave relative arrival times as the source wave travels within the stratigraphic profile. This is typically done by identifying reference points or markers within the seismograms (e.g., maximum peaks/troughs or crossovers) or through techniques that implement the cross-correlation function or the cross-power spectrum.

In both the DST and CST investigations, there are site conditions that result in wave multiples referred to as TIRs, which make the estimation of interval relative arrival times a very difficult task. TIRs are typical in CST investigations (since horizontally traveling source waves have high angles of incidence on bounding stratigraphic layers), whereas in DST investigations, TIRs are encountered whenever there are significant man-made structures nearby the test location.

The processing of seismograms that contain TIRs requires BSDtv. BSDtv refers to the case where there is an unknown direct source wave and time-variant overlapping (reflected) source waves recorded by the seismogram. The goal of BSDtv is to separate the overlapping source waves. This paper has

outlined a BSDtv algorithm referred to as BSDSolver-tv. The BSDSolver-tv filter formulation builds upon a previously published technique in BSD referred to as PPD. The BSDSolver-tv applies the following *a priori* information for TIRs.

- Although the phase of the source wave changes for each reflection, the dominant frequency remains the same.
- The time width of the source wave remains constant.
- The reflected source waves are modeled as AMSs.
- The AMTs of the direct and reflected source waves remain constant.

Full details on the formulation and implementation of BSDSolver-tv algorithm are provided within this paper. An important component of the BSDSolver-tv algorithm is the modeling of the source wave as an AMS. The AMS is demonstrated to be a highly robust and accurate approximation for many analytical and real representations of seismic source waves. The implementation and performance of the BSDSolver-tv algorithm was demonstrated by considering very challenging synthetic seismograms. The seismograms were challenging due to the fact that there were five closely spaced overlapping source waves with equivalent reflection coefficient dipoles. It was shown that the BSDSolver-tv algorithm was able to obtain accurate estimates of the direct source wave and corresponding interval velocities for a VSP investigation. It is the intention of the authors to incorporate AMT0 data interpolation into the BSDSolver-tv algorithm so that the computational requirements are subsequently considerably reduced. The authors also plan on processing synthetic seismograms with TIRs and complicated measurement noise and real data with BSDSolver-tv algorithm and presenting the results in a future paper.

REFERENCES

[1] W. D. L. Finn, "Dynamic response analysis of soils in engineering practice," in *Mechanics of Engineering Materials*. Hoboken, NJ, USA: Wiley, 1984, ch. 13.

[2] R. D. Andrus, K. H. Stokoe, and R. M. Chung, "Draft guidelines for evaluating liquefaction resistance using shear wave velocity measurements and simplified procedures," Nat. Inst. Standards Technol., Gaithersburg, MD, USA, NIST IR 6277, 1999.

[3] K. Aki and P. G. Richards, *Quantitative Seismology*, 2nd ed. Sausalito, CA, USA: University Science Books, 2002.

[4] R. D. Andrus and and K. H. Stokoe, "Liquefaction resistance of soils from shear-wave velocity," *J. Geotech. Geoenviron. Eng.*, vol. 126, no. 11, pp. 1015–1025, Nov. 2000.

[5] R. G. Campanella, F. T. C. Robertson, and D. Gillespie, "Seismic cone penetration test," in *Proc. INSITU*, 1986, pp. 116–130.

[6] E. Baziw, "Digital filtering techniques for interpreting seismic cone data," *J. Geotech. Eng.*, vol. 119, no. 6, pp. 98–1018, Jun. 1993.

[7] R. F. Ballard, "Method for crosshole seismic testing," *Geotech. Eng. Div.*, vol. 102, no. GT12, pp. 1261–1273, Dec. 1976.

[8] A. Amini, "Application of seismic cone for characterization for ground improved by vibro-replacements," Ph.D. dissertation, Dept. Civil Eng., Univ. British Columbia, Vancouver, BC, Canada, 2006.

[9] A. Amini and J. A. Howie, "Numerical simulation of downhole seismic cone signals," *Can. Geotech. J.*, vol. 42, no. 2, pp. 574–586, Apr. 2005.

[10] E. Baziw and G. Verbeek, "Signal processing challenges when processing DST and CST seismic data containing TIRs," *Geotech. Testing J.*, submitted for publication.

[11] E. Baziw, "Derivation of seismic cone interval velocities utilizing forward model," *Can. Geotech. J.*, vol. 39, no. 5, pp. 1181–1192, Oct. 2002.

[12] E. Baziw, "Two and three dimensional imaging utilizing the seismic cone penetrometer," in *Proc. 2nd Geotech. ISC*, 2004, pp. 1611–1618.

[13] E. Baziw and G. Verbeek, "Deriving interval velocities from downhole seismic data," in *Geotechnical and Geophysical Site Characterization 4*, A. B. Huang and P. W. Mayne, Eds. Boca Raton, CA, USA: CRC Press, 2012, pp. 1019–1024.

[14] R. E. Sheriff and L. P. Geldart, *Exploration Seismology*, 1st ed. Cambridge, U.K.: Cambridge Univ. Press, 1982, pp. 117–119.

[15] J. M. Mende, *Optimal Seismic Deconvolution—An Estimation-Based Approach*. San Diego, CA, USA: Academic Press, 1983.

[16] J. M. Mendel, *Lessons in Estimation Theory for Signal Processing, Communications, and Control*. Englewood Cliffs, NJ, USA: Prentice-Hall, 1995.

[17] T. J. Ulrych and M. D. Sacchi, *Information-Based Inversion and Processing with Applications*, 1st ed. Amsterdam, The Netherlands: Elsevier, 2005.

[18] A. Gholami and M. D. Sacchi, "A fast and automatic sparse deconvolution in the presence of outliers," *IEEE Trans. Geosci. Remote Sens.*, vol. 50, no. 10, pp. 4105–4116, Oct. 2012.

[19] E. Baziw and T. J. Ulrych, "Principle phase decomposition—A new concept in blind seismic deconvolution," *IEEE Trans. Geosci. Remote Sens.*, vol. 44, no. 8, pp. 2271–2281, Aug. 2006.

[20] E. Baziw, "Implementation of the principle phase decomposition algorithm," *IEEE Trans. Geosci. Remote Sens.*, vol. 45, no. 6, pp. 1775–1785, Jun. 2007.

[21] E. Baziw, "Incorporation of iterative forward modeling into the principle phase decomposition algorithm for accurate source wave and reflection series estimation," *IEEE Trans. Geosci. Remote Sens.*, vol. 49, no. 2, pp. 650–660, Feb. 2011.

[22] T. Imai and K. Tonouchi, "Correlation of N-value with S-wave velocity and shear modulus," in *Proc. 2nd Eur. Symp. Penetration Testing*, Amsterdam, The Netherlands, 1982, pp. 57–72.

[23] E. Baziw and I. Weir-Jones, "Application of Kalman filtering techniques for microseismic event detection," *Pure Appl. Geophys.*, vol. 159, no. 1–3, pp. 449–473, Jan. 2002.

[24] E. Baziw, B. Nedilko, and I. Weir-Jones, "Microseismic event detection Kalman filter: Derivation of the noise covariance matrix and automated first break determination for accurate source location estimation," *Pure Appl. Geophys.*, vol. 161, no. 2, pp. 303–329, Feb. 2004.

[25] E. Baziw and G. Verbeek, "Passive (micro-) seismic event detection by identifying embedded "event" anomalies within statistically describable background noise," *Pure Appl. Geophys.*, vol. 169, no. 12, pp. 2107–2126, Dec. 2012.

[26] E. R. Kanasewich, *Time Sequence Analysis in Geophysics*, 3rd ed. Edmonton, AB, Canada: The Univ. of Alberta Press, 1981.

Erick Baziw (M'05–SM'08) received the B.A.Sc. degree in geophysics engineering, the M.A.Sc. degree in geotechnical engineering, and the Ph.D. degree in geophysics time series analysis from The University of British Columbia, Vancouver, BC, Canada, in 1986, 1988, and 2007, respectively.

He is currently a Managing Director of Baziw Consulting Engineers Ltd., Vancouver, BC, Canada. His research interests include Bayesian recursive estimation, signal processing, and imaging, with a particular emphasis on blind seismic deconvolution, passive seismology, site characterization, seismic tomography, and instrument modeling.

Dr. Baziw is a Registered Professional Engineer in the disciplines of geophysics and software engineering.

Gerald Verbeek received the B.Sc. degree in civil engineering and the M.Sc. degree in structural engineering from Delft University of Technology, Delft, The Netherlands, in 1981 and 1983, respectively.

He was an Adjunct Professor with the University of Texas at Tyler, Tyler, TX, USA, where he taught courses in civil engineering materials and construction standards. His research and professional interests focus on state-of-the-art, practical, and user-friendly applications of applied seismology techniques for engineering design and site characterization. He has authored or coauthored several papers and technical reports in these areas.

Mr. Verbeek is a member of several professional organizations, including the American Society for Testing and Materials and the D18 Committee on Soil and Rock, where he participates in the efforts to set industry standards for downhole seismic testing.